Carbon Monoxide Emissions from Electrolysis Process in EGA Smelters

Mohammad Al Jawi[1], Eiman Al Obaidli[2], Ramanathan Natesan[3], Shane Pollé[4], Mohamed Mahmoud[5], Kindle Williams[6], Alexis Fenton[6] and Albert Wu[6]

1. Senior Manager – Environment & Waste Management
2. General Superintendent - Environment
3. Supervisor Environment & Waste Management
4. Manager – Cell Lining and Environment Control
5. Manager – Centre of Excellence

Emirates Global Aluminium (EGA), Abu Dhabi, United Arab Emirates

6. Students, David H. Koch School of Chemical Engineering Practice, MIT

Corresponding author: maljawi@ega.ae

Abstract

Carbon monoxide (CO) is generated in the aluminium reduction process mainly by back reaction, leading to current efficiency loss. CO is also generated by the Boudouard reaction or so-called CO_2 burn of the anodes. These two reactions occur under the anode cover and crust. It has been most often assumed that the CO burns in the air nearly completely as soon as it emerges from below the crust and that the CO emissions from the potrooms and the gas treatment centres (GTCs) are negligible. However, measurements in EGA, which were set up to follow UAE Environment regulations, show that the CO emissions from the GTCs are typically from 800 to 1200 mg/Nm^3 (approximately 53 to 76 kg/t Al), which are well above the UAE Environment limit of 500 mg/Nm^3. This limit was set up on the basis of combustion processes, which can effectively control CO emissions; however, the ability for aluminium electrolysis processes to control CO emissions is much less understood. A three-part kinetic model was developed which accounts for chemistry in the bath, anode pores, and gas above bath, to better understand the reactions at hand. It is shown in the paper that the measured CO emissions can be understood from theory and cannot be decreased without significant changes to the current configuration of the smelting process. The CO measurement technique and equipment are also described.

Keywords: CO generation in aluminium electrolysis, CO emissions, back reaction, current efficiency loss, Boudouard reaction.

1. Introduction

Aluminium is produced through the Hall-Héroult process, in which aluminium is electrochemically reduced from alumina in a cryolite bath. Within this bath, the alumina is dissolved and aluminium ions migrate to the cathode, where they are reduced to molten aluminium metal. Oxygen (O_2) from alumina reacts with the consumable carbon anodes to form carbon dioxide (CO_2). In parallel, back reaction occurs according to Equation (1) in Section 2.1, to form carbon monoxide (CO). Various other reactions produce gaseous side products such as CO, hydrofluoric acid (HF), perfluorocarbons (PFCs), and sulphur dioxide (SO_2).

CO_2, CO (indirectly), and PFCs are contributors to climate change as greenhouse gases. Among these, CO is also toxic to humans, but this is of no concern in open areas such as smelters because its concentration is very low for the amounts emitted by the stack. CO is generated both by back reaction of aluminium with CO_2 occurring in the bath and by the Boudouard reaction occurring under the anode cover and crust. It has usually been assumed that whatever CO is generated under the anode cover completely combusts in the air under the hood and, consequently, that the CO emissions from the Hall-Héroult process are negligible. However, measurements made by EGA,

required by UAE Environment regulations, show that CO emissions range typically from 800 to 1200 mg/Nm^3, starkly disagreeing with conventional understanding of CO emissions from aluminium smelting. EGA CO measurements are shown in Figure 1. Given this large discrepancy between experimental values and conventional understanding, we set out to gain better understanding of CO emissions generated in aluminium smelting and emitted to the atmosphere. After employing a third-party assessment of CO emissions in the aluminium industry, it was found that no other aluminium smelter worldwide has attempted to manage their CO emissions, nor has any other governmental agency instituted CO regulations for smelters. Given this, we set out to fundamentally understand the factors that contribute to CO emissions and the theoretical and realistic level of CO emissions from aluminium smelting.

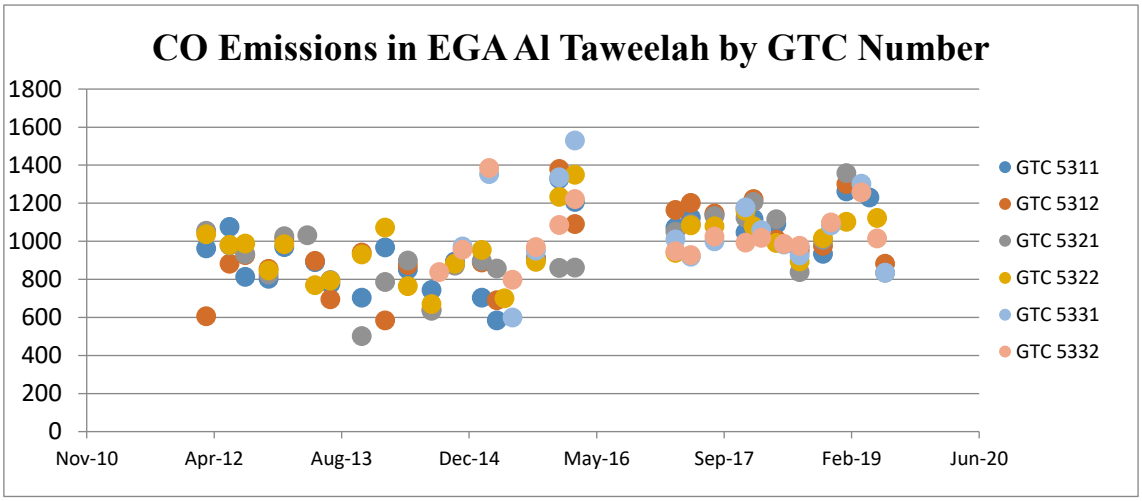

Figure 1. CO emissions measurements in EGA Al Taweelah

Our efforts resulted in a three-part kinetic model that fundamentally explains the generation of CO in the bath and the anode pores, as well as its consumption in the gas space above the bath. The results of this model are in agreement with measured values, providing insight into the nature of CO emissions and demonstrating that, unfortunately, these emissions cannot be decreased without significant changes to the current configuration of the smelting process. As such, we believe that this model is a first step towards better understanding of CO emissions in aluminium smelters.

This work is the result of collaboration between EGA and Massachusetts Institute of Technology (MIT), David H. Koch School of Chemical Engineering Practice wherein a team of three MIT students spent one month at EGA to work on the project of CO emissions.

2. Methodology

The kinetic model, constructed in MATLAB, was divided into three modules: the electrolyte bath, the porous anode, and the “above-bath” space. These divisions capture the regimes where the physics are most distinct from one another. In a first-pass approach to the model, many simplifying assumptions were made within each of these modules, which were relaxed when possible. The priority when developing the model was to estimate the minimum CO emissions that might reasonably be expected of an aluminium cell. As such, the simplifying assumptions made in the development of the model were each selected so that the exiting CO concentration was underestimated.

The inputs to the bath module are parameters only; this module is independent of the anode and "above-bath" modules. The outputs of the bath, however, are the exiting CO_2 and CO flow rates, which inform both the anode and "above-bath" modules. Exit flow rates from the anode are a further input to the "above-bath" module, from which final outlet concentrations are obtained.

2.1. "Bath" Module

One of the primary routes to CO generation in aluminium smelting – as well as the primary loss of current efficiency in a cell – is the back reaction of aluminium with CO_2:

$$2Al(l) + 3CO_2(g) = 3CO(g) + Al_2O_3(diss.) \quad (1)$$

This reaction takes place within the electrolyte bath, in the space between the anode and the cathode, as illustrated in Figure 2 [1]. Typically, the rate of this reaction depends on how well the liquid aluminium dissolved in the bath is able to get in contact with CO_2 bubbles. As such, the reaction is often swifter when the anode-cathode distance (ACD) is small, meaning that CO_2 is generated in close proximity to the aluminium pad and the aluminium can easily travel to CO_2 bubbles. However, this is not always the case, as magnetohydrodynamic (MHD) instability is also a large contributor to the upward transport of aluminium. In order to properly model this regime, diffusion of dissolved aluminium was considered. It was assumed on the first pass through the model that temperature within the bath was uniform and constant at 960 °C, and that laboratory correlations between cell conditions and back reaction rate could be applied to industrial smelters. Due to the complexity of the bath chemistry and unpredictable nature of MHD instability, these assumptions were not relaxed.

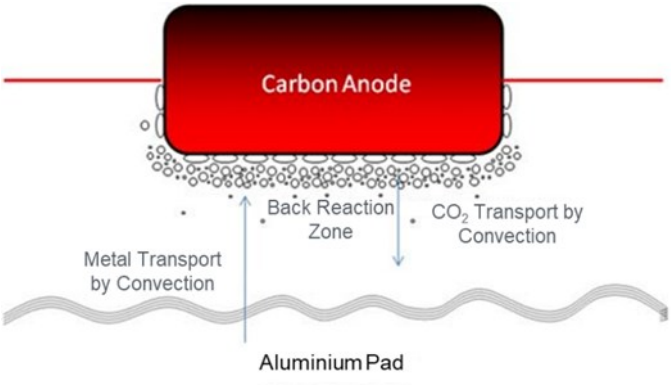

Figure 2. Diagram of the space between the anode and cathode, where the back reaction takes place [1].

Another reaction for which it would be useful to account in the bath modelling is electrochemical CO production:

$$C(s) + O^{2-}(diss.) = CO(g) + 2e^- \quad (2)$$

wherein oxygen from dissociated alumina adsorbs to the carbon anode and oxidation occurs electrochemically. This reaction occurs at a standard potential of $E° = 1.02$ V, and although it is not widely addressed in the literature, it was deemed a point of interest as a CO source, along with other electrochemical side-reactions [2, 3]. As documented in Section 3, due to lack of literature kinetic data, side electrochemical reactions were ultimately neglected in the final model.

2.2. Anode Module

Within the porous anode, it is hypothesized that there are two primary methods of CO generation – the Boudouard reaction on the bath side and air burn on the hood side. In the Boudouard reaction, CO_2 generated in the bath diffuses into the porous network of the anode and undergoes a surface reaction to form CO. In the air burn reaction, atmospheric oxygen diffuses similarly into the top of the anode, forming CO and CO_2 through incomplete and complete combustion reactions. These reactions and their locations are summarized in Figure 3.

The thermodynamics of both the Boudouard and air burn reactions are well understood; for the Boudouard reaction as written here, the reaction favours CO_2 at low temperatures and CO at approximately 975 °C. Since the bottom of the anode is approximately at bath temperature (960 °C), CO formation is favoured. The air burn reactions are spontaneous under all conditions, but the kinetics of this reaction are unknown. Consequently, the amount of CO or CO_2 generated is unknown.

The method to model the transport of species and their reactions within the anode was to treat the arrangement as two independent, one-dimensional steady-state reaction-diffusion systems – one at the bath side considering only the Boudouard reaction and the other at the hood side considering only the air burn reactions. For example, at the bath side, CO_2 enters the system from the boundary and reacts/diffuses through the pores according to the kinetics, forming CO, which diffuses out. The outputs of the model are the molar flow rates in/out of the system for all species, to be used as inputs into the "above-bath" module. The system at the top of the anode for air burn was built similarly.

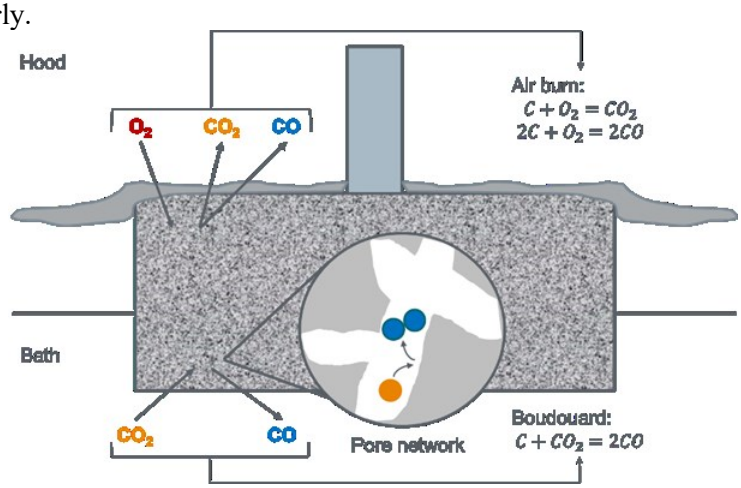

Figure 3. Summary of reactions considered in the anode module.

2.3. "Above-bath" Module

The "above-bath" module is different from both the bath and anode modules, as there is only one reaction being considered, which is purely chemical (i.e., involving no electric potentials or pores), and is described in Equation (3).

$$2CO\ (g) + O_2\ (g) = 2CO_2\ (g) \tag{3}$$

Hence, the "above-bath" module simply considers the thermodynamics and chemical kinetics governing the reaction described above, using the outputs from the previous two modules as inputs.

The first step of developing this module was to find an adequate rate law for the reaction. Brokaw [4] derived a rate law for the generation of CO_2 (and hence the consumption of CO), which is given in Equation (4). The derivation of the rate law can be found in Brokaw [4].

$$r = k_i[\mathrm{CO}][\mathrm{O_2}] + k_6[\mathrm{CO}]\left\{\left(\frac{k_i[\mathrm{CO}][\mathrm{O_2}]}{k_{1'}[\mathrm{H_2}] + k_6[\mathrm{CO}]}\right)\left[\cosh(\lambda t) - 1 + \frac{\lambda}{k_{2'}[\mathrm{O_2}]}\sinh(\lambda t)\right]\right\} \quad (4)$$

Where λ is described below in Equation (5).

$$\lambda = \left[\frac{2k_{2'}[\mathrm{O_2}](k_{3'}[\mathrm{H_2}] + k_5[\mathrm{H_2O}])(k_{1'}[\mathrm{H_2}] + k_6[\mathrm{CO}])}{k_{1'} + k_{3'}[\mathrm{H_2}] + k_5[\mathrm{H_2O}] + k_{2'}[\mathrm{O_2}] + k_6[\mathrm{CO}]}\right]^{\frac{1}{2}} \quad (5)$$

Here, lower case "k_n"s represent the reaction rate constants for the elementary reactions listed in Brokaw (m^3/mol-s), the bracketed terms are concentrations (mol/m^3), and "t" represents time (s). This model was used to calculate the rate of consumption for CO_2 at a given temperature. CO combustion was modelled along the path of the blue arrow in Figure 4.

It was also assumed that no CO reacts under and within the crust (from the "bath top level" to the bottom of the blue arrow in Figure 4), as there is almost no oxygen present in this part of the pot [5]. In addition, the resulting CO emissions from all five breaker holes were averaged to give the mean CO emissions coming out of a typical pot.

The distance along the blue arrow was discretized, and the information provided by EGA modelling team was splined. Since the distance and velocity along the length of the blue arrow were known, the amount of time spent in each step could be calculated. Average reaction conditions at each discretized point (e.g., temperature, pressure, velocity) were provided from computational fluid dynamics (CFD) data, and within each step the degree of CO conversion to CO_2 was calculated using the kinetic model from Brokaw [4]. Only four species (CO, O_2, H_2O, and CO_2) were assumed, and the ideal gas law was used. In our calculations, we did not account for the formation of hydrogen (H_2), nor of HF, which undergoes side reactions with water.

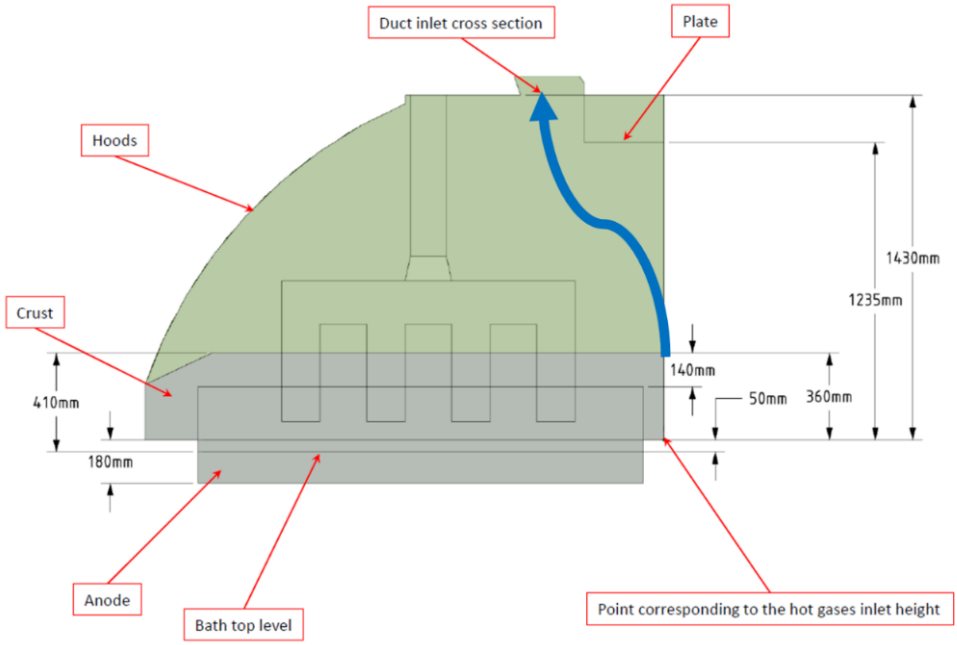

Figure 4. Geometrical set-up of CO reaction above the crust of the smelting pot per EGA modelling team [5].

3. Results and Discussion – Module Development

3.1. Electrolyte Bath Module

The chemistry of the bath which is relevant to the production of CO can be broadly broken down into electrochemical reactions and the so-called "back reaction." The former category includes a variety of processes – particularly anodic half-reactions – which compete with the primary process occurring in the cell (formation of CO_2). Due to lack of kinetic parameters in the existing smelting literature (confirmed by [6, 7]), these are not incorporated in the final version of the model. However, the reactions themselves can be found in other publications [2, 3].

The "back reaction" is accounted for below by implementing a kinetic model developed in 2015 [8]. It was confirmed with the author that, save for the specifics of the mass transfer coefficient, this model should hold true for contemporary industrial cell designs [6].

3.1.1. Electrochemical Reactions

The primary electrochemical half-reaction at the cathode is

$$4Al^{3+}\ (diss.) + 12e^{-} = 4Al\ (l) \tag{6}$$

while the corresponding half-reaction on the anode is

$$6O^{2-}\ (diss) + 3C\ (s) = 3CO_2\ (g) + 12e^{-} \tag{7}$$

Notably, neither of these reactions occurs exactly in this form; the aluminium-containing ions are aluminium fluorides (AlF_6^{3-} and AlF_4^{-}), while the oxygen-containing ions are likely $Al_2O_2F_4^{2-}$ and $Al_2OF_6^{2-}$ [9].

It is fairly straightforward to account for the emissions resulting from the electrochemical processes if it is assumed that these are the only half-reactions taking place. Because Na^+ ions are not observed to discharge at the cathode, this assumption is fairly safe for the cathodic half-reaction under normal cell operating conditions [9]. However, a variety of other reactions, including many which are more thermodynamically favourable than the formation of CO_2, may occur at the anode [2]. It was desired to account for these reactions by treating the cell as an equivalent electrical circuit in which parallel reactions could be treated as parallel impedance elements at each anode surface [10]. However, in order to do this, a fundamental mechanistic understanding was needed, but no detailed electrokinetic parameters were found for the reactions in question. The absence of such understanding was confirmed with experts in the field, and is noted as an active area of interest [6, 7, 9, 11, 12]. As rate constants for other steps in the potential mechanisms, such as adsorption and desorption, were unknown, these values were thought to be calculable through transition state theory (TST) analysis. Due to the number of assumptions made regarding the mechanisms of the anodic half-reactions, this analysis was not pursued to completion.

As a result of these restrictions, it is assumed in the model that 100 % of the current passing through a cell contributes to generating aluminium and carbon dioxide. Notably, this assumption also ignores reductions in current efficiency through the presence and redox cycling of such impurities as P, S, and Si [13]. However, these reactions do not directly affect CO output, and moreover are relatively small contributors to current efficiency reduction.

For 100 % current efficiency to CO_2, the following generation rates are obtained for EGA Al Taweelah DX Technology at 418 kA and DX+ Technology at 465 kA:

Table 1. Primary reaction product generation based on 100 % CE in EGA Al Taweelah.

Species	DX (418 kA)	DX+ (465 kA)
CO_2	1.08 mol/s	1.20 mol/s
Al	1.44 mol/s	1.61 mol/s

3.1.2. Back Reaction

The back reaction, or recombination of CO_2 and aluminium to form alumina and CO, proceeds as mentioned previously in Equation (1). It has been well-established in literature that the rate of this back reaction is diffusion-limited [8, 14, 15, 16]. The primary reactions governing dissolution of aluminium are as follows:

$$3NaF + Al = 3Na + AlF_3 \quad (8)$$

$$AlF_3 + 2Al = 3AlF \quad (9)$$

Since these reactions are diffusion-limited, any kinetic model accounting for the back reaction must take mass transfer into consideration. One such model was developed in 1994 by Solli [14], but was found to be outdated, significantly overpredicting current efficiencies for the industrial process [14, 16]. As such, this model was replaced with one developed on the lab scale for conditions which are more relevant to today's industrial smelters [8].

The back-reaction model takes in bath temperature and composition as well as cathodic current density. Using these parameters, it calculates current efficiency assuming the back reaction is the only loss of aluminium, and subsequently how much CO is generated due to this efficiency loss. It

should also be noted that this model likely underestimates CO generation, as the mass transfer coefficient is likely larger than what we used due to MHD phenomena, sludge formation, and other such large-scale effects.

For the two technologies analysed herein, the outputs from the bath module alone were as follows:

Table 2. Outputs of bath module for the two EGA Al Taweelah pot technologies investigated.

	DX (418 kA)	DX+ (465 kA)
Current Efficiency	94.1%	94.1%
CO Outlet Flow Rate	0.129 mol/s	0.143 mol/s
CO_2 Outlet Flow Rate	0.955 mol/s	1.062 mol/s

If it were assumed that no further reactions involving CO occurred after the bath module, but dilution by ambient air in the space above the bath were still considered (air flow = 2.82548 kg/s), these outputs would yield an exit CO concentration of 1657 mg/Nm^3.

3.2. Anode Module

The anode module, based on the chemistry described in Section 2, was modelled by: (1) determining the diffusion regime and consequently calculating the diffusion coefficient; (2) setting up the system of differential equations and boundary conditions, (3) solving this system of equations, and (4) yielding the boundary fluxes and molar flow rates. These steps in the approach are described in detail below.

3.2.1. Determination of Diffusion Regime and Calculation of Diffusion Coefficient

The first step towards modelling the transport within the anode was to establish the correct diffusion regime, allowing for usage of the correct diffusion coefficient depending on the system state. This is done through the calculation of a Knudsen number, the ratio of the mean free path of a molecule (λ) to the average pore diameter (d_p), i.e., λ/d_p [17, 18]. The Knudsen number describes three diffusion regimes depending on its value, shown in Figure 5.

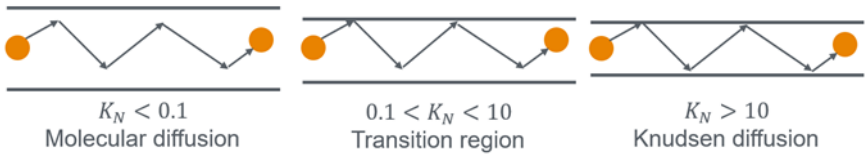

Figure 5. Three diffusion regimes described by the Knudsen number. The path for all three cases is the same, only the pore diameter is changing.

For the bath side, the Knudsen number for both CO_2 and CO was calculated to be approximately 0.3. For the hood side, the Knudsen number was approximately 1. Since this indicates both molecular and Knudsen diffusion are occurring for both sides of the anode, both molecular and Knudsen diffusion coefficients needed to be calculated and combined to find the apparent diffusion coefficient using the Chapman-Eksong approximation and fundamental kinetic theory. The porosity and tortuosity of the anode also had to be accounted for (estimated to be 0.2 and 1.5, respectively) [19], resulting in an effective diffusion coefficient for each species. The system of differential equations could then be set up.

3.2.2. Set up the Boundary Conditions and Differential Equations

In order to solve the reaction-diffusion system, boundary conditions and the reaction rate must first be specified. For the bath side, since the system is solving for the concentration profiles of CO_2 and CO as well as the temperature profile, six boundary conditions must be specified (two for each variable). For the hood side, the system solves for the concentration profiles of O_2, CO, and CO_2, and the temperature profile, meaning eight boundary conditions are needed.

For the bath side, the temperature on the bath-side surface was set to 960 °C. Further, CO_2 bubbles exert a hydrostatic pressure of approximately 4 kPa on the anode surface, establishing the second boundary condition [20]. The pressure of CO on the surface of the anode was estimated from the relative production of CO to CO_2 in the bath and was found to be approximately zero via a ratio analysis between pressures and concentrations. It was also reported that on the bath side, the reaction only occurs in the first 30 mm from the surface, establishing the length of the system as well as the remaining 3 boundary conditions [21]. The rate found describes the rate of carbon consumption [22], and a visual representation of these boundary conditions is presented in Figure 6.

$$\text{Rate of C consumption (mol/s)} = r = \frac{e^{16.9}}{60}\exp\left(-\frac{207\,000}{RT}\right)(1-x)C_{CO_2,0}\ [22] \qquad (10)$$

For the hood side, one significant difference is the presence of the anode cover, which is used to insulate the anode and protect it from air reactions. The thickness was set to 70 mm [23]. Since there is no reaction occurring in the cover, the concentration profile of all gases within the cover is linear. Outside in the hood, the pressures of the three gases was set to atmospheric levels. The appropriate boundary condition at the anode surface (z = 0) is then, taking O_2 as an example:

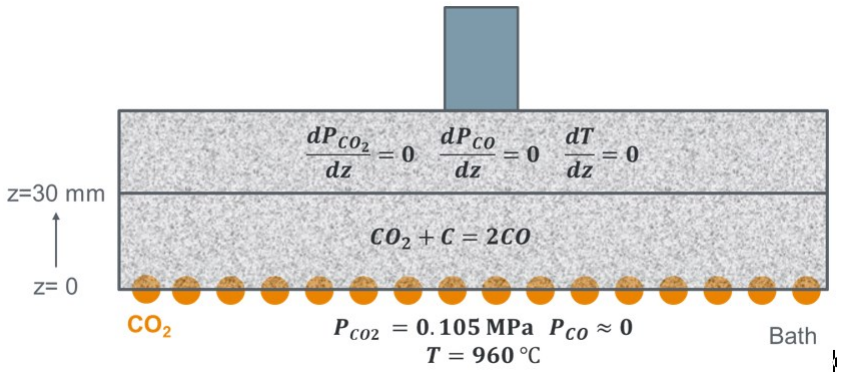

Figure 6. Geometry of the bath-side system with boundary conditions.

$$P_{O_2}(z=0) + \frac{dP_{O_2}}{dz}(z=0) \times -70\ \text{mm} = 0.21\ \text{atm} \qquad (11)$$

Similar equations set the first three boundary conditions. Additionally, the temperature of the anode surface under the cover was set to 770 °C [23]. Further, on the hood side, the reaction occurs only in the first 30 mm from the surface, again establishing the length of the system as well as the remaining 4 boundary conditions. [21] The rate found for CO and CO_2 describe rates of generation [24], and a visual representation of these boundary conditions is found in Figure 7.

$$\text{Rate CO generation (mol/s)} = r_{CO} = \frac{10^{6.4}}{15}\exp\left(-\frac{131\,000}{RT}\right)(1-x)P_{O_2}^{\ 1.6}\ [24] \tag{12}$$

$$\text{Rate } CO_2 \text{ generation (mol/s)} = r_{CO_2} = \frac{10^{4.2}}{15}\exp\left(-\frac{98\,000}{RT}\right)(1-x)P_{O_2}^{\ 0.8}\ [24] \tag{13}$$

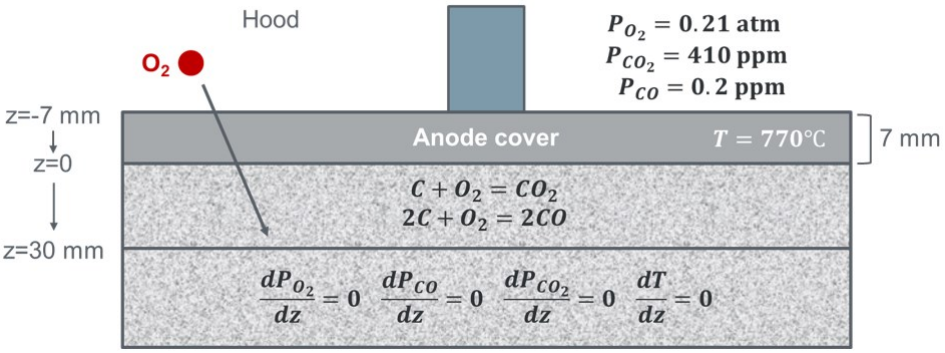

Figure 7. Geometry of the hood-side system with boundary conditions.

Consequently, based on the derived boundary conditions, the reaction-diffusion system of equations for the bath side is:

$$D_{eff,CO_2}\frac{d^2C_{CO_2}}{dz^2} - r\left(C_{CO_2},T\right) = 0 \tag{14}$$

$$D_{eff,CO}\frac{d^2C_{CO}}{dz^2} - 2r\left(C_{CO_2},T\right) = 0 \tag{15}$$

$$\kappa\frac{d^2T}{dz^2} - \Delta H_{\text{rxn}}\left(C_{CO_2},T\right) = 0 \tag{16}$$

Where κ is the thermal conductivity in W/m-K [23] and ΔH_{rxn} is the heat of reaction in J/mol [25], both as a function of temperature. ΔH_{rxn} for this reaction is endothermic for all temperatures.

For the hood side, the system of equations is:

$$D_{eff,O_2}\frac{d^2C_{O_2}}{dz^2} - \frac{1}{2}r_{CO}\left(C_{CO_2},T\right) - r_{CO_2}\left(C_{O_2},T\right) = 0 \tag{17}$$

$$D_{eff,CO}\frac{d^2C_{CO}}{dz^2} - r_{CO}\left(C_{CO_2},T\right) = 0 \tag{18}$$

$$D_{eff,CO_2}\frac{d^2C_{CO_2}}{dz^2} - r_{CO_2}\left(C_{CO_2},T\right) = 0 \tag{19}$$

$$\kappa\frac{d^2T}{dz^2} - \Delta H_{CO}r_{CO}\left(C_{CO_2},T\right) - \Delta H_{CO_2}r_{CO_2}\left(C_{O_2},T\right) = 0 \tag{20}$$

Where κ is the thermal conductivity [23] and ΔH_{CO} and ΔH_{CO2} are the heat of reactions [8] as stated above, both as a function of temperature. Both reactions are exothermic for all temperatures.

The temperature dependence of the anode thermal conductivity was kindly provided by Alexander Arkhipov [23], and the temperature dependence of heats of reaction were found by fitting ΔH data from JANAF tables [25].

Both systems of equations were solved using MATLAB. The concentration and temperature profiles for both systems are shown in Figures 8–9.

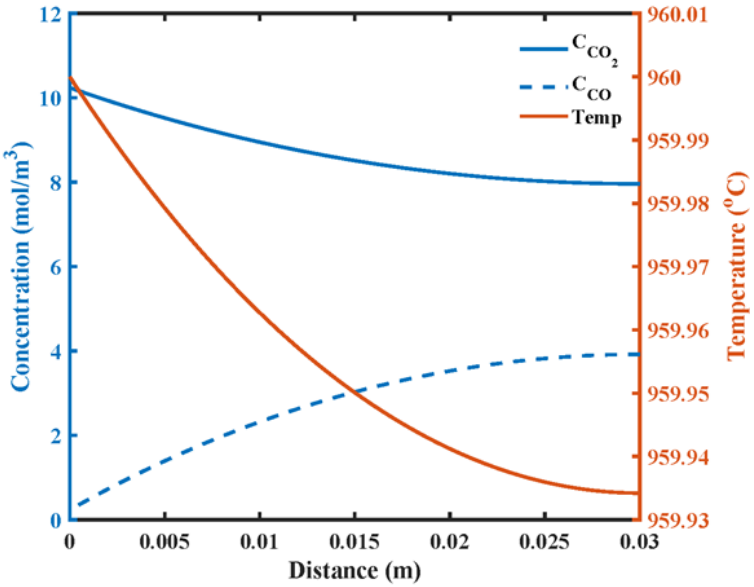

Figure 8. Concentration and temperature profiles for the bath-side system of the anode. The x-axis corresponds to Figure 6; the anode is at x = 0.

It is important to note that at z = 0, the anode cover / anode interface, the system transitions from reaction and diffusion occurring within the anode (z = 0 to z = 30 mm) to only diffusion occurring within the cover (z = -70 mm to z = 0). The diffusion in the cover is linear and the profile satisfies the boundary conditions specified above at z = -70 mm. As such, the results match intuition.

3.2.3. Calculate Boundary Fluxes and Molar Flow Rates

To determine the steady-state molar flow rates in and out of the system, the boundary fluxes had to first be calculated, at z = 0. When multiplied by the anode surface area for anodes in DX+ cells, the molar flow rates could be found. For example:

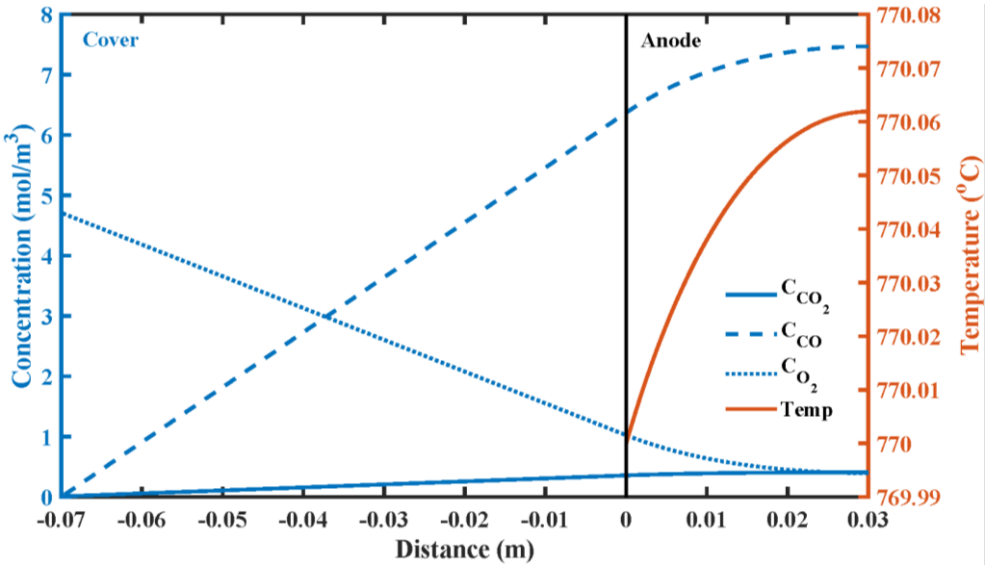

Figure 9. Concentration and temperature profiles for the hood-side system of the anode. The x-axis corresponds to Figure 7; the anode is at x = 0.

$$\left[-D_{eff}\frac{dC}{dz}\right]_{z=0}(\text{mol/m}^2\text{-s-anode})\times SA_{anode}(\text{m}^2)=\text{molar flow rate (mol/s-anode)} \quad (21)$$

$$\rightarrow F_{CO_2,anode}=8.1392\times10^{-5}\ \text{mol/s-anode}$$

$$\rightarrow F_{CO,anode}=-1.6296\times10^{-4}\ \text{mol/s-anode}$$

Similarly, for the hood side, the molar flow rates were calculated similarly as previously by first calculating the boundary fluxes at z = -70 mm and multiplying by the anode surface area.

$$\left[-D_{eff}\frac{dC}{dz}\right]_{z=-70\text{ mm}}(\text{mol/m}^2\text{-s-anode})\times SA_{anode}(\text{m}^2)=\text{molar flow rate (mol/s-anode)} \quad (22)$$

$$\rightarrow F_{O_2,anode}=2.9936\times10^{-5}\ \text{mol/s-anode}$$

$$\rightarrow F_{CO,anode}=-5.6817\times10^{-5}\ \text{mol/s-anode}$$

$$\rightarrow F_{CO_2,anode}=-2.4838\times10^{-6}\ \text{mol/s-anode}$$

It is important to note that these flow rates are with respect to the anode system; e.g. a positive flow rate means flow into the system, and a negative flow rate means flow out of the system. This is accounted for during model integration, and the flows are made with respect to the "above-bath" module. Note that the magnitudes of these flow rates are much smaller than those coming out of the electrolyte bath and are negligible.

3.3 "Above-bath" Module

3.3.1 "Above-bath" Model Validation

The first step in the "above-bath" module was to validate the kinetic model proposed by Brokaw [4] against relevant experimental data found in Li et al. [26] and originally obtained by Yetter, Dryer and Rabitz [27]. The kinetic model was first compared to data obtained under excess O_2 conditions. The results are shown in Figure 10.

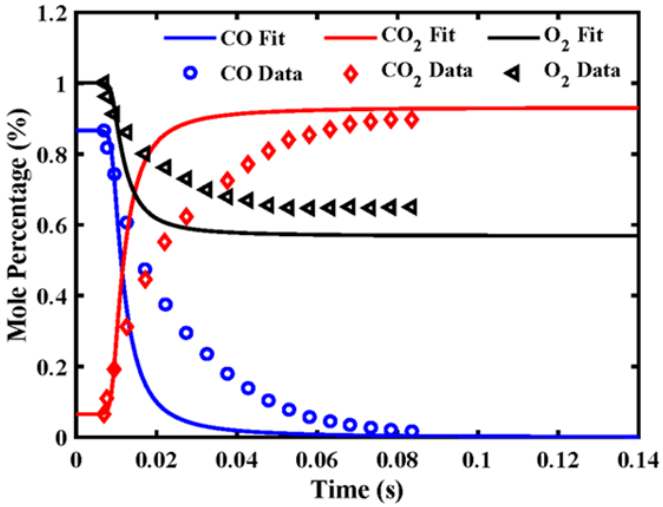

Figure 10. Validation of Brokaw [4] with experimental data from Li et al. [26] for high O2 content, with shifted data to match initiation time steps with the model.

At early times of the reaction, the model predicts a faster rate of CO consumption than illustrated in the experimental data. However, this overestimate of the consumption rate will provide an underestimate of the outlet concentration of CO from the smelting pot, providing a lower bound on the CO emissions. While the fits are not perfect, this model is in strong agreement with experimental data despite its simplicity (only six elementary reactions are considered) and provides a better fit to the data than more complex models considered. A similar analysis was performed for a mixture of CO and O_2 where CO was in excess. The comparison of the model to the shifted data is found in Figure 11.

The rates appear to match up well in this example at small times. The fit of the model to experimental data is remarkable at early reaction times. However, there appears to be a discrepancy in mole percentages at equilibrium. This said, the agreement is remarkable given the simplicity of the model. Although the model and the validation data do not match perfectly, based on the mole fraction error at equilibrium (max absolute error 8.2 %), we are confident that the proposed rate law approximates the kinetics and the thermodynamics of the reaction well enough to be applied to smelters.

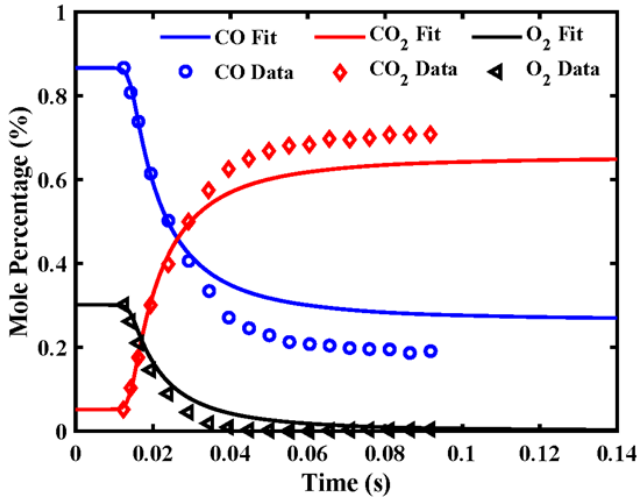

Figure 11. Validation of Brokaw [4] with experimental data from Li et al. [26] for low O2 content, with shifted data to match initiation time steps with the model.

3.3.2. Main Simulation, Results, and Discussion

Given this validation, a simulation was run to attempt to duplicate output measured emissions values. The results are depicted in Figure 12. For our model, the CO emissions concentration of ~1150 mg CO/Nm^3 was achieved when the ambient temperature was 30 °C and relative humidity 60 %. Note in this figure that concentrations are normalized to exit stream dilution to de-convolute the effects of dilution from that of reaction.

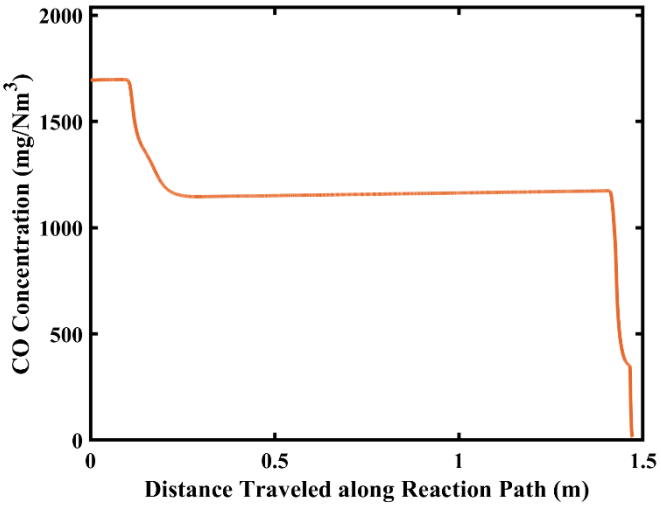

Figure 12. Concentration profile of CO, in mg/Nm^3, along the length of the path travelled according to Figure 4.

In Figure 12, the CO primarily reacts between 10 and 20 cm along its path, and afterwards remains comparatively flat at a concentration of ~1150 mg/Nm^3. At the end of the reaction path, the concentration drops off to zero very rapidly, due to a stagnation point in the fluid velocity (the remainder of the CO stream exits the duct in the direction perpendicular to the plane of the page in Figure 4).

We also found that the model was very sensitive to relative humidity and ambient air temperature. As such, the effects of these factors on output CO concentrations were also explored and are reported in Table.

Table 3. Analysis of CO emission concentration with changes in ambient temperature and humidity. Both humidity and ambient temperature are varied.

Relative Humidity (%)	Ambient Temperature (°C)	CO Emissions (mg/Nm^3)
40	30 (approximate yearly mean)	1289
50	30	1230
60	30	1166
70	30	1102
80	30	1042
Relative Humidity (%)	**Ambient Temperature (°C)**	**CO Emissions (mg/Nm^3)**
60 (estimated mean)	20	1322
60	25	1251
60	35	1044
60	40	909

It should be noted that the average relative humidity and temperature of air in Dubai is 60 % at 30 °C, and as such, these were the baseline conditions used for this study. Two things should be noted: (1) the air entering the hood is closer to 55 - 60 °C, but this difference in temperature has no effect on the simulated results. The ambient conditions are only needed to determine the mole fraction of water in the air entering the hood. We assume the water mole fraction in air does not significantly change as the air temperature elevates to 55 - 60 °C, so we use ambient air humidity and temperature for simplicity. Further, (2) the local water mole fraction within the hood may be lower than that in air. Alumina in the anode cover may act as a desiccant, and hydrogen bonding with HF may also lower the effective humidity. However, these effects can only be quantified with humidity and temperature measurements under the hood, which can help refine the simulation results. Elementary reactions involving HF can also be studied for model improvement.

We also observed that the CO emissions output increased along with the fineness of the discretized mesh; further tests are required to find the optimum mesh size.

Ultimately, the "above-bath" module reports CO emission concentrations that are within the range of the actual readings from the aluminium pots. As such, we believe that this module, as well as the overall model, successfully captures the dominant physical processes affecting CO emissions for a typical aluminium smelter at EGA and can be used to further investigate the dynamics of CO emissions.

4. Recommendations

4.1 Model Improvements

Foremost among recommendations emerging from this project is model validation. In particular, it is recommended to verify that the process conditions of the pot match the parameters assumed by the model.

The analysis provided here is a starting point for rigorous scientific accounting of CO formation during smelting, but by no means is it comprehensive or complete. The following observations may offer a starting place for refinement:

To improve the bath module, it is recommended that fundamental research into the mechanisms behind anodic reactions continues and the resulting electrokinetic parameters be properly implemented. The electrochemical analysis should also be extended to impurity ions known to be parasitic to current – for instance, Phosphorus-containing species. It is also recommended that tests similar to those done by Solheim [8] be carried out in an industrial-scale cell to properly account for the mass transfer differences related to the back reaction due to system size. To improve the anode module, it is recommended to conduct kinetic experiments on the rates of reaction for the Boudouard reaction and the two air burn reactions to improve model accuracy. Finally, to improve the "above-bath" module, it is recommended to investigate the effects HF will have on the oxidation of CO to CO_2 by considering elementary reactions between HF and CO, CO_2, H_2O, and O_2 . The effects of alumina in scrubbing water vapour from the air should also be investigated to determine how much water vapour is removed by the anode cover to more accurately quantify the concentration of water vapour under the hood.

4.2 CO Emissions Management

Based on the outcomes of a model sensitivity analysis, it appears that an influential parameter for CO emission is relative humidity of air under the hood. For the range of relative humidities studied, the model confirms that the measured values in the smelter of 800 to 1200 mg/Nm^3 are to

be expected and can be explained by the major reactions occurring within the model smelting pots.

5. Conclusions

A kinetic model accounting for reactions in an aluminium electrolysis cell was developed, with particular attention to the emission of CO from the process. The three-part model accounts for reactions in the electrolyte bath, inside the pores of the anodes, and in the gas above the bath. Many assumptions went into the generation of this model; these are partially documented in this report. It was determined that a range of ambient air conditions (e.g., 40 - 80 % relative humidity and 20-40 °C) corresponded to the measured emissions of 800 – 1200 mg CO/Nm^3. Therefore, the primary recommendation is process validation of the amount of water available to react with CO, along with further model refinement as the kinetics of reactions involving water inside the hood are investigated. Through a sensitivity analysis of model parameters, it was found that the model was most sensitive to bath temperature and composition, current, and the relative humidity and temperature of ambient air. The smelting operation parameters are optimised for best pot performance and cannot be manipulated for reducing CO emissions, while the relative humidity and temperature of the ambient air around most smelters cannot be controlled. With additional model validation and further refinement, it is likely that the cell model developed herein will be a useful tool for understanding the CO emissions from aluminium smelters.

6. Acknowledgements

We would like to thank the teams at EGA and MIT for taking the time to provide all necessary information. In particular, we would like to thank Vinko Potocnik for very helpful and informative discussions and the EGA modelling team, Alexander Arkhipov, Ievgen Necheporenko, and Alexander Mukhanov, for providing CFD model set up, parameters, and results for our validation. We would also like to thank Dr. Mohamed Mahmoud, Muhammad Aqeel, Omar AlMheiri, and Satish Ranjalkar for the large amount of work done to coordinate the station of MIT students at EGA and ensure the necessary resources to pursue this project were provided. Lastly, we would like to thank the external professionals contacted, Asbjørn Solheim, Prof. Donald Sadoway, and Dr. Alton Tabereaux, for their insight into the current state of the smelting literature.

The group would also like to thank the station director, Dr. Brian Stutts, for his mentorship, as well as everyone on the MIT Practice School team for their support and encouragement.

7. References

1. http://www.aluminum-production.com/current_efficiency.html, retrieved on 19 July 2019.
2. Ruth A. Roberts and Phillip J. Ramsey, Evaluation of fluorocarbon emissions from the aluminum smelting process, *Light Metals* 1994, 1007-1014.
3. Barry Welch, Controlling laws – part 2: Mass and energy balance, *The University of Auckland - Postgraduate Certificate in Light Metals Reduction*, 2016.
4. Richard S. Brokaw, Ignition kinetics of carbon monoxide-oxygen reaction, *NASA Technical Note*, Washington, D.C., 1966.
5. Ievgen Necheporenko, EGA internal communication - CFD results of aluminium electrolysis pots, Dubai, UAE, 2017.
6. Asbjørn Solheim, personal correspondence, 2017.
7. Donald Sadoway, personal correspondence, 2017.

8. Asbjørn Solheim et al., Current efficiency in laboratory aluminium cells, *Proceedings of 33rd International ICSOBA Conference*, 29 November – 1 December 2015, Dubai, UAE, Paper AL14, *Travaux* 44, 625-634.
9. Warren E. Haupin, Electrochemistry of the Hall-Heroult process for aluminum smelting, Journal of Chemical Education, Vol. 60, No. 4, (1983), 279-282.
10. Karthish Manthiram, personal communication, 2017.
11. Alton Tabereaux, personal correspondence, 2017.
12. Mark M. R. Dorreen et al., Influence of heat transfer on anode reactions when electrowinning metal from its oxides dissolved in molten fluorides, *Journal of the Electrochemical Society*, Vol. 164, No. 8, (2017), H5108-H5118.
13. Geir Martin Haarberg, Effects of electrolyte impurities on the current efficiency during aluminium electrolysis, *Proceedings of 33rd International ICSOBA Conference*, 29 November – 1 December 2015, Dubai, UAE, Paper AL27, *Travaux* 44, 761-767.
14. Per A. Solli et al., A laboratory study of current efficiency in cryolitic melts, *Light Metals* 1994, 195-203.
15. Shiva Prasad, Studies on the Hall-Heroult aluminum electrowinning process, *Journal of the Brazilian Chemical Society*, Vol. 11, No. 3, (2000), 245-251.
16. Barry Welch, Martin Iffert and M. Skyllas-Kazacos, Applying fundamental data to reduce the carbon dioxide footprint of aluminum smelters, *JOM*, Vol. 60, No. 11, 2008, 17-24.
17. Troy Lee Hudson, Growth, diffusion, and loss of subsurface ice on Mars: experiments and models, *CalTech Thesis*, (2008), 16-28.
18. Barry A. Sadler and S. H. Algie, A porosimetric study of sub-surface carboxy oxidation in anodes, *Light Metals*, (1991), 594-605.
19. Stein Rørvik and Lorentz Petter Lossius, Measurement of tortuosity of anode porosity by 3D micro x-ray computed tomography, *Proceedings of 35th International ICSOBA Conference*, Hamburg, Germany, 2017, Paper CB13, *Travaux* 46, 757-766.
20. Khalil Khaji and Mohammed Al Qassimi, The role of anode manufacturing processes in net carbon consumption, *Metals*, Vol. 6, No. 128, (2016).
21. Uthaiporn Suriyapraphadilok et al., Anode butt cores: physical characterization and reactivity measurements, *JOM*, Vol. 57, No. 35, (2005), 35-41.
22. F. Chevarin et al., Characterization of carbon anode constituents under CO_2 gasification: a try to understand the dusting phenomenon, *Fuel*, Vol. 156, (2015), 198-210.
23. Alexander Arkhipov, EGA internal data, 2017.
24. Chao'en Li and Trevor C. Brown, Carbon oxidation kinetics from evolved carbon oxide analysis during temperature-programmed oxidation, *Carbon*, Vol. 39, (2001), 725-732.
25. NIST, *NIST-JANAF thermochemical tables*, Available at: http://kinetics.nist.gov/janaf/.
26. Juan Li et al., A comprehensive kinetic mechanism for CO, CH2O, and CH3OH combustion, *International Journal of Chemical Kinetics*, Vol. 39, No. 3, (2007), 109-136.
27. R. A. Yetter, F. L. Dryer and H. Rabitz, A comprehensive reaction mechanism for carbon monoxide/hydrogen/oxygen kinetics, *Combustion Science and Technology*, Vol. 79, (1991), 97-128.